Epitaxial p-type SiC as an efficient self-driven photocathode for water splitting

Masashi Kato[a,*], Tomonari Yasuda[a], Keiko Miyake[a], Masaya Ichimura[a] and Tomoaki Hatayama[b]

[a]*Dept. of Engineering Physics, Electronics and Mechanics, Nagoya Institute of Technology, Gokiso, Showa, Nagoya 4666-8555, Japan*

[b]*Graduate School of Materials Science, Nara Institute of Science and Technology, 8916-5 Takayama, Ikoma, Nara 630-0192, Japan*

Solar-to-hydrogen conversion efficiencies of water-splitting photochathodes using epitaxially grown p-type 4H-, 6H- and 3C-SiC were estimated in a two-electrode system without applying any external bias. By using electrode materials with small oxygen overpotentials as counter electrodes, the photocurrent became comparable to that observed in a three-electrode system with a suitable bias. Estimated efficiencies seem to depend on the bandgap of the SiC polytypes. For the 3C-SiC, the obtained efficiency was 0.38%, which is so far the highest value reported for SiC. We confirmed that the hydrogen volumes estimated from the photocurrent were almost the same as actual volumes observed by gas chromatography.

Keywords: SiC, photochathode, water-splitting, conversion efficiency

*Corresponding author.
Dept. of Engineering Physics, Electronics and Mechanics, Nagoya Institute of Technology,
Gokiso, Showa, Nagoya 4666-8555, Japan
Tel. & Fax: +81-52-735-5581
E-mail address: kato.masashi@nitech.ac.jp

1. Introduction

Hydrogen production by water splitting is attracting attention as a next-generation energy technology [1-8]. There are several techniques used for water splitting such as thermal decomposition, photobiology, photocatalysis and photoelectrochemistry. Among these, the photoelectrochemical method is an environment-friendly process [7,8]. However, for commercially viable photoelectrochemical water splitting technology, the solar-to-hydrogen conversion efficiencies must be significantly increased and corrosion of the photoelectrodes avoided. One of the popular approaches is to utilize metal oxides as photoelectrodes owing to their resistance to corrosion. However, their band gaps are usually too large to absorb most of the solar light [9]. Semiconductor materials other than metal oxides sometimes show high conversion efficiencies, but they have weak resistance against corrosion [10,11]. Thus, new materials, such as nitride compounds, are being investigated to develop photoelectrodes exhibit both high conversion efficiencies and high resistance to corrosion [6,12,13]. Also, studies on silicon carbide (SiC) as a photoelectrode material have been conducted [14-19]. We have previously reported on the capability and durability of p-type SiC for water splitting applications [17-19]. Among the SiC polytypes, 3C-SiC is expected to show the highest efficiency because it has the lowest band gap of 2.3 eV. The band gaps of the 4H- and 6H-SiC polytypes are 3.2 and 2.9 eV, respectively—higher than that of 3C-SiC. For this reason, 3C-SiC is capable of absorbing a significant part of the visible light compared with the other polytypes. Generally, the epitaxial SiC layer shows a larger photocurrent than the bulk SiC crystal [18,19]. Owing to these characteristics and observations, epitaxially grown p-type 3C-SiC is attractive as a durable and efficient photocathode for water splitting.

Most of the studies on SiC's water splitting properties have used the three-electrode system during photoelectrochemical measurements and efficiencies have been estimated only from measured photocurrents in the three-electrode system [14-17]. In the three-electrode system, external electrical power is supplied from a potentiostat to stabilize the potential in SiC. Therefore, the two electrode-system is still required to estimate the actual solar-to-hydrogen conversion efficiencies [18,19]. Additionally, when estimating the efficiencies from a photocurrent, it is generally assumed that the Faraday efficiencies are 100% [14-19]. However, this is not always the case. Hence confirmation of the actual efficiencies is needed and can be determined by direct observation of the hydrogen volumes. In this study, the photocurrents from p-type SiC in the two-electrode system using various counter electrodes are first measured. Then, to estimate the Faraday efficiency, the solar-to-hydrogen conversion efficiencies of epitaxially-grown p-type 4H-, 6H- and 3C-SiC are obtained from both the measured photocurrents and the hydrogen volumes.

2. Experiment Description

Samples employed in this study were epitaxially grown p-type 4H-, 6H- and 3C-SiC. Two 4H-SiC (p4H and less-N_A), 6H-SiC (p6H) and 3C-SiC (p3C) samples were used in the study. (The text inside the parentheses refers to the sample labels and will be mentioned in the discussion.) The 4H-SiC sample was grown on a (0001) Si-face with 8° off-oriented 4H-SiC substrates. The 6H- and 3C-SiC samples were grown on a (0001) Si-face with 3.5° off-oriented and on-axis 6H-SiC substrates, respectively. (Please note that generally for homoepitaxial growth of SiC, substrates off-oriented from the (0001) Si-face are preferable [20]). The epitaxial layer thicknesses and doping densities estimated by the capacitance–voltage (*C*–*V*) measurements are listed in Table 1. Ohmic contacts were fabricated on the samples by sintered Al or Al/Ti/Ni particles and the contacts were connected to a wire. The sample surface was immersed and exposed to the electrolyte and the rest of the sample was covered by wax or sealed with an O-ring. For the three-electrode system, Pt and a saturated calomel electrode (SCE) with a salt bridge to the electrolyte

were used as counter and reference electrodes, respectively. For photocurrent observation, the applied potential was adjusted to 0 V vs. SCE. In *C–V* measurements, the potential was swept with 1 kHz oscillation. For the two-electrode system, several counter electrode materials were used and no external power was supplied. Metals and RuO_2 were employed as counter electrodes. We used RuO_2 because some metals may be oxidized or dissolved during hydrogen generation. Oxidation and dissolution of the counter electrode may cause chemical bias to the hydrogen generation, and RuO_2 is a stable material for oxidation with a small oxygen overpotential [21,22]. By using RuO_2, a photocurrent can be obtained without any chemical biases. Schematics of the three- and two-electrode systems are shown in Figs. 1(a) and 1(b), respectively. All experiments were conducted using an aqueous solution containing 1 mol/L H_2SO_4 at room temperature. A solar simulator with power of 1 W/cm^2 was used as a light source for photocurrent observation. For hydrogen volume observation, a sealed cell was employed with the two-electrode system using a Ni counter electrode. Photocurrents were observed, and after illumination, the evolved gas was extracted using a syringe. The hydrogen content was then estimated by gas chromatography.

3. Results and discussion

Figure 2 shows the time dependence of photocurrents for p4H, p6H and p3C in the three-electrode system. The photocurrents are constant and seem to depend on the band gap of the SiC polytypes; 3C-SiC has the smallest band gap and exhibits the largest photocurrent among the all samples. As for epitaxial 4H-SiC [18], p6H shows a larger photocurrent than that of the bulk 6H-SiC crystals reported in Ref. 18. This could be due to the wider depletion layers and longer electron diffusion lengths in the epitaxial layers than in the bulk crystals. Possible effects due to depletion layer width and electron diffusion length will be addressed in a future publication.

Figure 3 shows the time dependence of photocurrents for p4H, p6H and p3C in the two-electrode system using either Pt or Ni as counter electrodes. When Pt was used as a counter electrode, the photocurrents were very small compared to those obtained in the three-electrode system. These results suggest that the adjustment of the potential difference between Pt and the electrolyte by the potentiostat enhances the photocurrent. On the other hand, for the Ni counter electrode, the measured photocurrents are larger than those obtained in the same system with the Pt electrode and are just as large as those in the three-electrode system.

Figure 4 shows the time dependence of photocurrents for less-N_A in the two-electrode system using various counter electrodes. As depicted in the figure, the photocurrents vary with the type of counter electrode, i.e., the photocurrent depends on the type of materials used as the counter electrode. Photocurrents are very small for the Pt and Au electrodes, while for the Cu, Ni and RuO_2 electrodes, the photocurrents are relatively large. In RuO_2, during the initial 400 s, the photocurrent decreased with time. This initial decrease of the photocurrent would be due to the weak physical bond between the RuO_2 and the glass substrate. This is because after the experiment, part of the RuO_2 peeled away or was removed from the glass substrate. RuO_2 was formed by sputtering on the glass substrate and during the experiment oxygen bubbles were observed to peel the RuO_2. However, after this initial decrease and until the end of the measurement, the photocurrent was stable and RuO_2 conducted the photocurrent generated in the SiC. Figure 5 depicts the photocurrent densities measured for various counter electrodes 600 s after starting the illumination against the reported oxygen overpotentials at 5 mA/cm^2 [21-23]. Pt and Au have relatively large oxygen overpotentials, while Ni, Cu and RuO_2 have small oxygen overpotentials. Therefore, to obtain a large photocurrent, the counter electrode should have relatively small oxygen overpotentials. Since the Ni and Cu photocurrents are comparable to that with RuO_2, the chemical bias effects would be negligible and the holes generated in the SiC would have the energy to overcome the oxygen overpotentials at the counter electrodes. This result suggests that with a suitable counter electrode,

epitaxial p-type SiC works as an efficient self-driven photocathode and the photocurrent would be limited by the characteristics of the SiC photocathodes.

The conversion efficiencies were estimated from the observed photocurrents 600 s after starting the illumination in the two-electrode system using Ni as the counter electrode. The solar-to-hydrogen conversion efficiency η can be obtained from

$$\eta\ (\%) = \frac{I \times 1.23}{L} \times 100\,, \qquad (1)$$

where I is the photocurrent, L is the light intensity and 1.23 represents the redox potential width between H^+/H_2 and O_2/H_2O. The results are listed in Table 1. p3C shows the largest η of 0.38% among the all samples. This η value is nearly four times larger than the value in our previous report using p-type 4H-SiC and is so far the highest among those reported for SiC. In fact, the thicknesses and net acceptor concentrations among the samples are different. Samples with a thick layer and low net acceptor concentration show a high η value because the increase in the light absorption layer and the electric field in the wide depletion layer enhance the number of electrons from the SiC to the electrolyte. Thus, it is difficult to discuss the quantitative differences among the polytypes.

Hydrogen volumes were evaluated by gas chromatography for p4H, p6H and p3C as shown in Fig. 6. The curves in Fig. 6 are the hydrogen volumes estimated from the measured photocurrents. For p3C, experiments were repeated for 15, 30 and 60 min to confirm the stability of the sample. For p4H, the observed hydrogen volume is much smaller than that expected from the photocurrent, which may have been caused by our experimental setup; when the hydrogen volume was small, hydrogen bubbles stuck to the electrolyte bath. The p3C exhibits a slight variation in the photocurrents for different durations: 15, 30 and 60 min. This difference could be caused by the non-constant exposure of the sample to the electrolyte in the cell, i.e., bubbles frequently stuck to the sample from the start and until the end of the experiments. Though p3C shows a slight variation in the photocurrents, the observed hydrogen volumes for p6H and p3C are similar to those estimated from the photocurrents. Values for η, estimated by time integration of the photocurrents up to 3600 s, are listed in Table 1. Therefore, most of the conducting electrons reduced the hydrogen ions and generated hydrogen gas (with a Faraday efficiency above 80%) and the η value of 0.38% (for the p3C sample) estimated from Eq. (1) is reliable.

4. Conclusions

We estimated the solar-to-hydrogen conversion efficiencies of epitaxially grown p-type 4H-, 6H- and 3C-SiC as water splitting materials. An efficiency of 0.38% for 3C-SiC was estimated from the measured photocurrent without external biases, and the reliability of this efficiency is supported by gas volume observation. Epitaxial p-type 3C-SiC can be considered as a promising self-driven photocathode material for water splitting applications.

Acknowledgements

This work is supported by Grant-in-Aid for Scientific Research 25107516, the JGC-S Scholarship Foundation and the Adaptable and Seamless Technology Transfer Program, Japan Science and Technology Agency.

[1] Grochala W, Edwards PP. Thermal decomposition of the non-interstitial hydrides for the storage and production of hydrogen. Chem. Rev. 2004;104:1283–316
[2] Akkermana I, Janssenb M, Rochac J, Wijffels RH. Photobiological hydrogen production: photochemical efficiency and bioreactor design. Int. J. Hydrogen Energy 2002;27:1195–208
[3] Maeda K, Domen K. Photocatalytic water splitting: recent progress and future challenges. J. Phys. Chem. Lett. 2010;1:2655–61.
[4] Bard AJ, Fox MA. Artificial photosynthesis: solar splitting of water to hydrogen and oxygen. Acc. Chem. Res. 1995;28:141–5.
[5] Tryk DA, Fujishima A, Honda K. Recent topics in photoelectrochemistry: achievements and future prospects. Electrochimica Acta 2000;45:2363–76.
[6] Khaselev O, Turner JA. A monolithic photovoltaic-photoelectrochemical device for hydrogen production via water splitting. Science 1998;280:425–7.
[7] Turner JA. Sustainable hydrogen production. Science 2004;305;972−4
[8] Bak T, Nowotny J, Rekas M, Sorrell CC. Photo-electrochemical hydrogen generation from water using solar energy. Materials-related aspects. Int. J. Hydrogen Energy 2002;27:991–1022
[9] Khan SUM, Al-shahry M, Ingler WB Jr. Efficient photochemical water splitting by a chemically modified n-TiO_2. Science 2002;297:2243–5.
[10] Mau WH, Huang CB, Kakuta N, Bard AJ, Campion A, Fox MA, White M, Webber SE. H_2 Photoproduction by Nafion/CdS/Pt Films in H_2O/S_2^- Solutions. J. Am. Chem. Soc. 1984;106:6537–42.
[11] Fujii K, Karasawa T., Ohkawa K. Photoelectrochemical Properties of InGaN for H_2 Generation from Aqueous Water. Jpn. J. Appl. Phys. 2005;44:7433–5.
[12] Fujii K, Ohkawa K. Bias-Assisted H_2 Gas Generation in HCl and KOH Solutions Using n-Type GaN Photoelectrode. J. Electrochem. Soc. 2006;153:A468–71.
[13] Aryal K, Pantha BN, Li J, Lin JY, Jiang HX. Hydrogen generation by solar water splitting using p-InGaN photoelectrochemical cells. Appl. Phys. Let. 2010;96:052110.
[14] Akikusa J, Khan SUM. Photoelectrolysis of water to hydrogen in p-SiC/Pt and p-SiC/ n-TiO_2 cells. Int. J. Hydrogen Energy, 2002;27:863–70.
[15] Liu H, She G, Mu L, Shi W. Porous SiC nanowire arrays as stable photocatalyst for water splitting under UV irradiation. Mater. Res. Bull. 2012;47:917–20.
[16] He C, Wu X, Shen J, Chu PK. High-efficiency electrochemical hydrogen evolution based on surface autocatalytic effect of ultrathin 3C-SiC nanocrystals. Nano Lett. 2012;12:1545–1548.
[17] Yasuda T, Kato M, Ichimura M. Characterization of Photoelectrochemical Properties of SiC as a Water Splitting Material. Mater. Sci. Forum 2012;717:585–8.
[18] Yasuda T, Kato M, Ichimura M, Hatayama T. SiC photoelectrodes for a self-driven water-splitting cell. Appl. Phys. Lett. 2012;101:053902.
[19] Yasuda T, Kato M, Ichimura M, Hatayama T. Solar-to-Hydrogen Conversion Efficiency of Water Photolysis with Epitaxially Grown p-Type SiC. Mater. Sci. Forum 2013;740:859–62. (Net acceptor concentrations listed in this reference were nominal values estimated from a reference sample. We corrected them by listing the concentrations estimated from C–V measurements in the H_2SO_4 solution in Table 1.)
[20] Kimoto T, Itoh A, Matsunami H. Step-Controlled Epitaxial Growth of High-Quality SiC Layers. Phys. Status Solidi (b) 1997;202:247–62.
[21] Lyons MEG, Floquet S. Mechanism of oxygen reactions at porous oxide electrodes. Part 2—Oxygen evolution at RuO_2, IrO_2 and $Ir_xRu_{1-x}O_2$ electrodes in aqueous acid and alkaline solution. Phys Chem Chem Phys 2011;13:5314–35.
[22] Trasatti S. Electrocatalysis by oxides—Attempt at a unifying approach. J. Electroanal. Chem. 1980;111:125–31.
[23] National Research Council, West CJ. International critical tables of numerical data, physics, chemistry and technology Vol.VI. McGraw-Hill Book Co., New York;1926:p340.

Figure captions

Fig. 1. Schematic of (a) the three-electrode system, and (b) the two-electrode system.

Fig. 2. Time dependence of photocurrents for p4H, p6H and p3C in aqueous H_2SO_4 solution with the three-electrode system.

Fig. 3. Time dependence of photocurrents for p4H, p6H and p3C in aqueous H_2SO_4 solution with the two-electrode system using Pt or Ni counter electrodes.

Fig. 4. Time dependence of photocurrents for less-N_A in aqueous H_2SO_4 solution with the two-electrode system using various counter electrodes.

Fig. 5. Photocurrents at 600 s after starting the illumination for less-N_A against oxygen overpotentials for the counter electrode in aqueous H_2SO_4 solution with the two-electrode system.

Fig. 6. Volumes of generated hydrogen at the unit-illuminated area in SiC in the two-electrode system. Curves are estimated volumes from photocurrents, while plots indicate observations by gas chromatography.

η and net acceptor concentrations obtained from C–V measurements and estimated η for the samples.

Sample	p4H	less-N_A	p6H	p3C
Polytype	4H	4H	6H	3C
Thickness (μm)	10	10	20	20
Net acceptor concentration (cm^{-3})	3×10^{16}	5×10^{14}	2×10^{16}	3×10^{16}
η estimated from photocurrent at 600 s (%)	0.10	0.20	0.26	0.38
η estimated from time-integrated (0–3600 s) photocurrent in the sealed cell (%)	0.08	Not measured	0.20	0.33

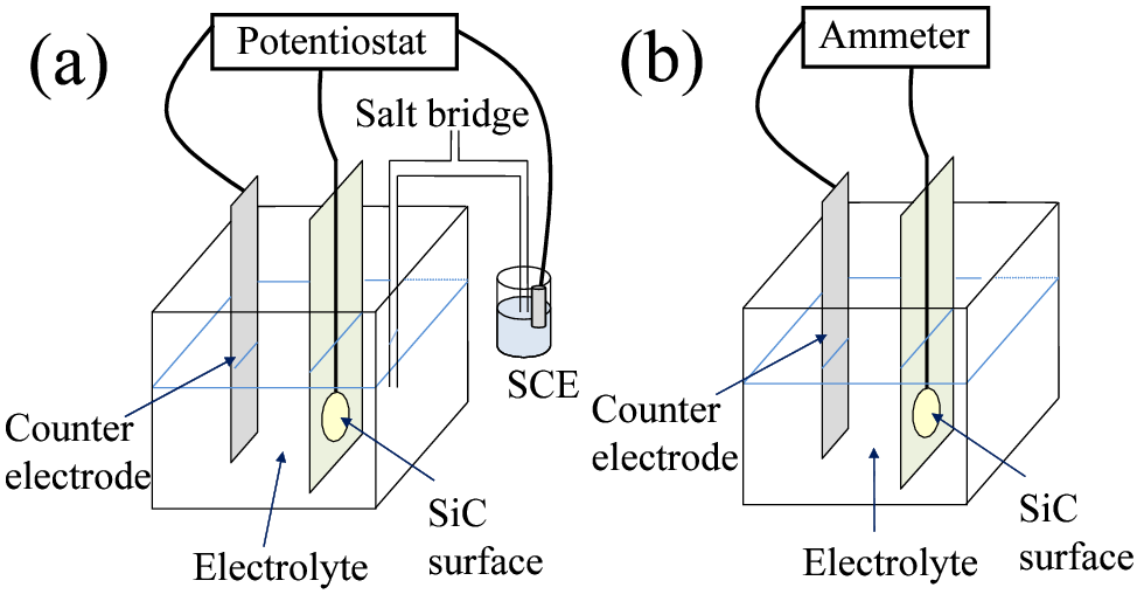
(a)
Potentiostat
Salt bridge
SCE
Counter
electrode
SiC
surface
Electrolyte
(b)
Ammeter
Counter
electrode
SiC
surface
Electrolyte

Fig.1

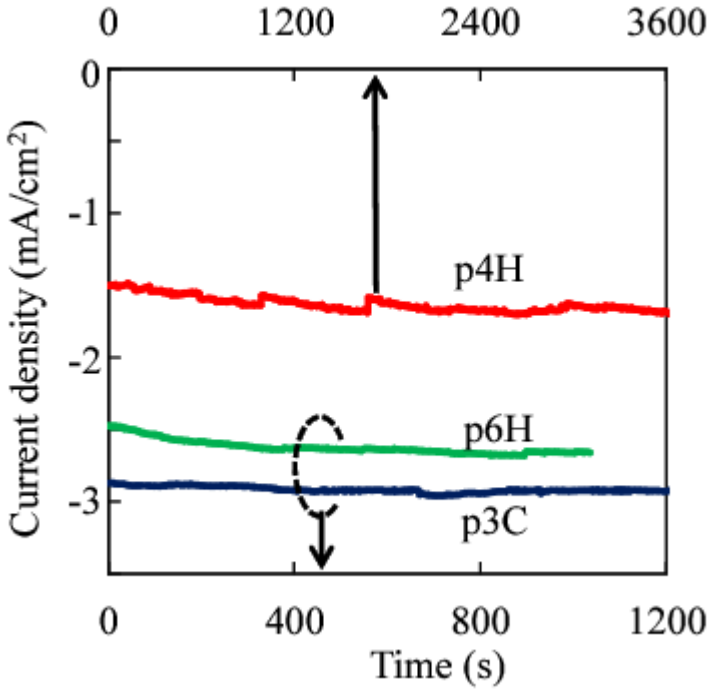
0
1200
2400
3600
0
-1
-2
-3
Current density (mA/cm²)
p4H
p6H
p3C
0
400
800
1200
Time (s)

Fig. 2

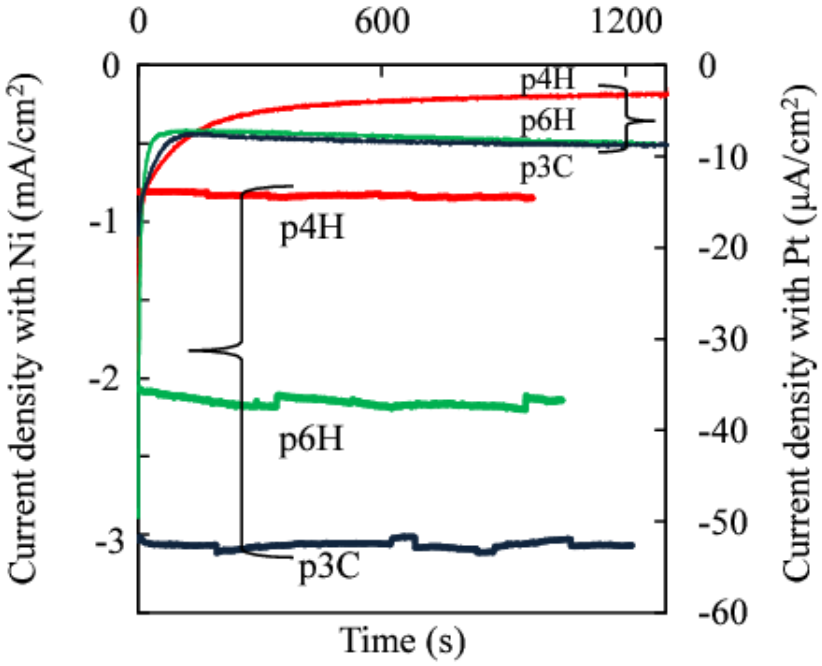
0
600
1200
0
-1
-2
-3
0
-10
-20
-30
-40
-50
-60
p4H
p6H
p3C
p4H
p6H
p3C
Current density with Ni (mA/cm²)
Current density with Pt (μA/cm²)
Time (s)

Fig. 3

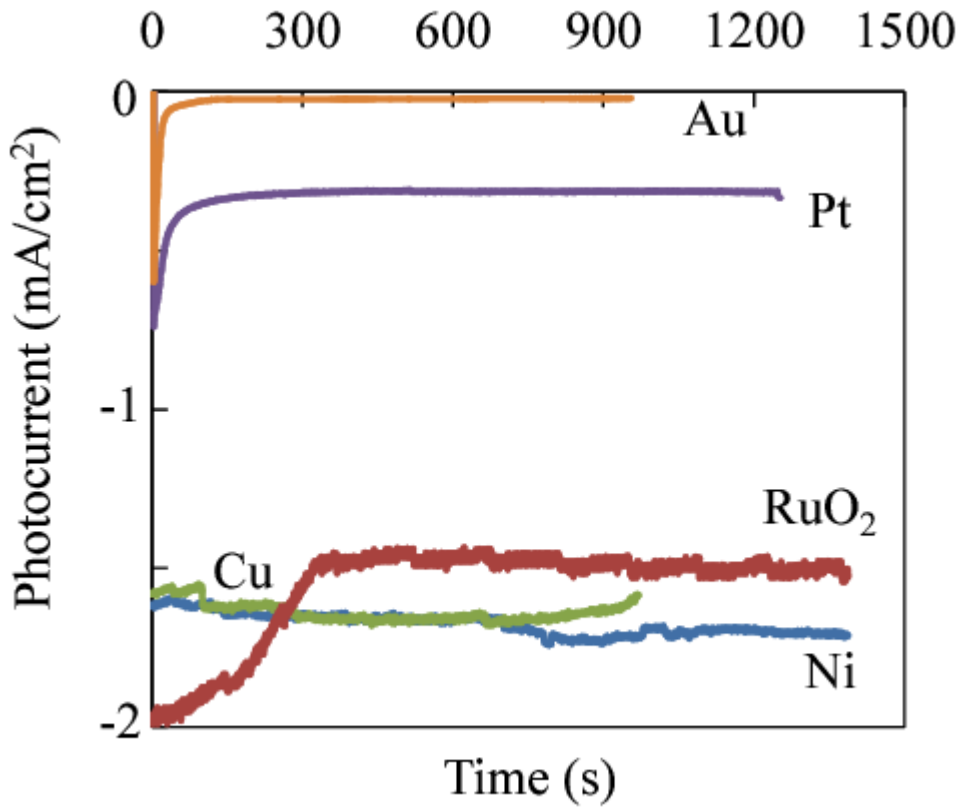
0
300
600
900
1200
1500
0
-1
-2
Photocurrent (mA/cm²)
Time (s)
Au
Pt
RuO2
Cu
Ni

Fig. 4

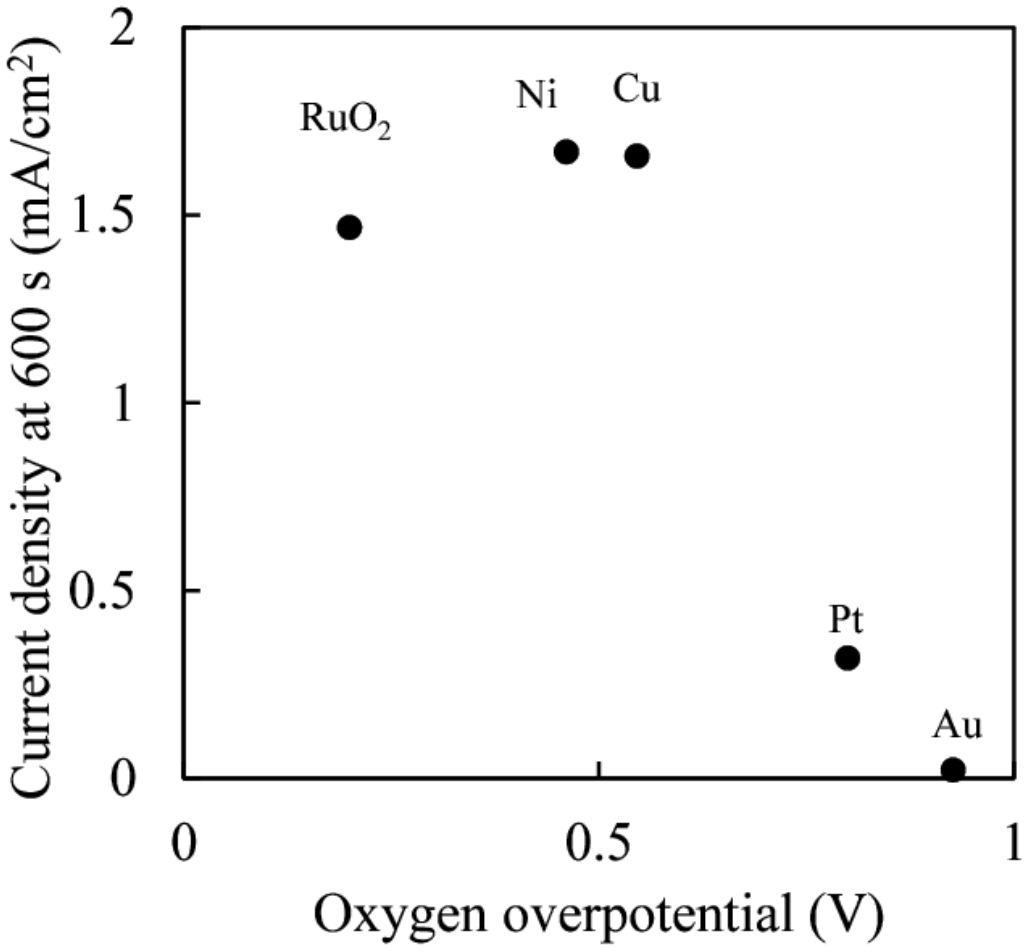
Current density at 600 s (mA/cm²)
2
1.5
1
0.5
0
0
0.5
1
Oxygen overpotential (V)
RuO2
Ni
Cu
Pt
Au

Fig. 5

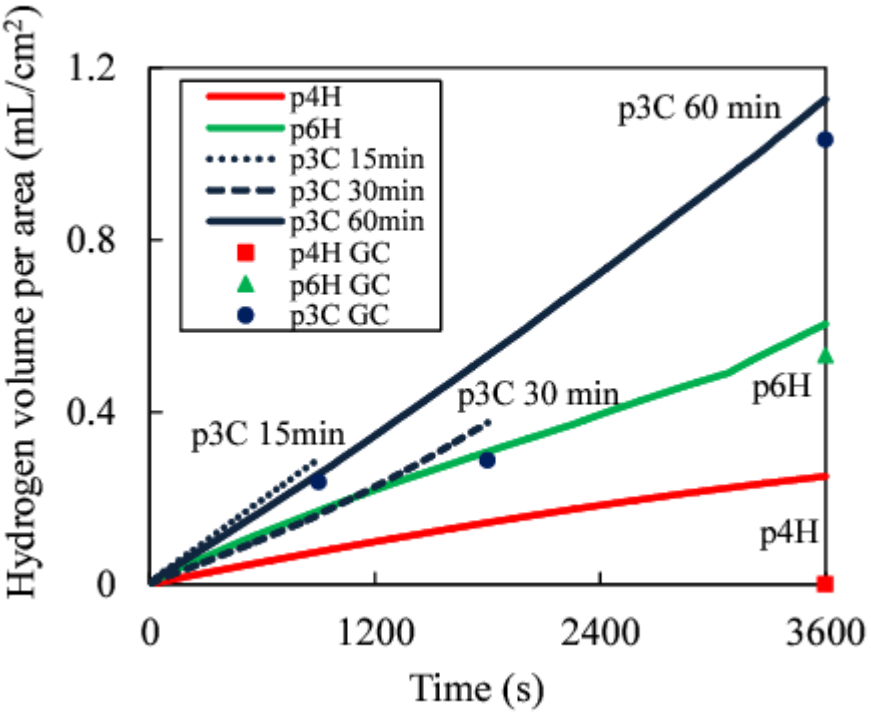
Hydrogen volume per area (mL/cm²)
1.2
0.8
0.4
0
0
1200
2400
3600
Time (s)
p4H
p6H
p3C 15min
p3C 30min
p3C 60min
p4H GC
p6H GC
p3C GC
p3C 60 min
p3C 30 min
p6H
p3C 15min
p4H

Fig. 6